lubricants

MDPI

Article

Effects of Intermetallic NiAl Particle Content on Friction and Wear of Spark Plasma-Sintered Alumina Matrix Composites

Nay Win Khun [1,2,*], Mingyue Huang [1], Zhong Alan Li [1,3], He Zhang [1], Khiam Aik Khor [1], Jinglei Yang [1,4] and Fei Duan [1]

[1] School of Mechanical and Aerospace Engineering, Nanyang Technological University, 50 Nanyang Avenue, Singapore 639798, Singapore; huangmy2025@gmail.com (M.H.); alanli@cuhk.edu.hk (Z.A.L.); zhanghe@scut.edu.cn (H.Z.); mkakhor@ntu.edu.sg (K.A.K.); maeyang@ust.hk (J.Y.); feiduan@ntu.edu.sg (F.D.)
[2] Institute of Microelectronics and Optoelectronics, Faculty of Electronics and Information Technology, Warsaw University of Technology, Koszykowa 75, 00-662 Warszawa, Poland
[3] Department of Biomedical Engineering, The Chinese University of Hong Kong, Hong Kong, China
[4] Department of Mechanical and Aerospace Engineering, Hong Kong University of Science and Technology, Hong Kong, China
* Correspondence: khunnaywin@gmail.com or nay_win.khun@pw.edu.pl

Abstract: The spark plasma sintering (SPS) technology was applied to develop alumina matrix composites (Al_2O_3MCs) with different nickel-aluminium (NiAl) particle contents of 5–20 wt.% to understand a correlation between their NiAl particle contents and their microstructures, fracture, hardness, friction, and wear. The incorporation of NiAl particles suppressed micrograins and micropores in the microstructures of the Al_2O_3MCs, which resulted in their improved fracture resistance. Increasing the NiAl particle content from 0 to 20 wt.% gave rise to a 23.9% decrease in the hardness of the Al_2O_3MCs. The Al_2O_3MCs had 18.2% and 13.3% decreases in their friction coefficients and 68.3% and 81.3% decreases in their specific wear rates under the normal loads of 2 and 6 N, respectively, with an increased NiAl particle content from 0 to 20 wt.% thanks to their decreased fatigue wear. The SPS Al_2O_3MCs with NiAl particles had promising tribological performance for rotating gas turbine components.

Keywords: spark plasma sintering; Al_2O_3 matrix composites; NiAl particles; hardness; friction; wear

check for updates

Received: 25 December 2024
Revised: 20 February 2025
Accepted: 22 February 2025
Published: 25 February 2025

Citation: Khun, N.W.; Huang, M.; Li, Z.A.; Zhang, H.; Khor, K.A.; Yang, J.; Duan, F. Effects of Intermetallic NiAl Particle Content on Friction and Wear of Spark Plasma-Sintered Alumina Matrix Composites. *Lubricants* **2025**, *13*, 101. https://doi.org/10.3390/lubricants13030101

Copyright: © 2025 by the authors. Licensee MDPI, Basel, Switzerland. This article is an open access article distributed under the terms and conditions of the Creative Commons Attribution (CC BY) license (https://creativecommons.org/licenses/by/4.0/).

1. Introduction

Ceramics have been widely used for gas turbine components working in extreme environments, where high temperature and mechanical strength are prerequisites because of their promising mechanical performance and high thermal resistance [1–3]. However, the relatively low fracture resistance of ceramics shortens their service life via surface fatigue failure when they are applied to rotating components [4].

Many monolithic materials do not possess the desired properties demanded by gas turbine components [5–7]. The development of composite materials can achieve outstanding structural and functional properties superior to those of monolithic materials [5–7]. Therefore, an incorporation of metallic particles in ceramic matrixes can produce ceramic matrix composites with improved fracture resistance but decrease their mechanical strength, such as elastic modulus and hardness [5–7]. Therefore, it is critical to select appropriate metallic reinforcements and proper production methods. Although Al_2O_3 and silicon carbide (SiC) are reportedly used for gas turbine components, Al_2O_3 has higher thermal and chemical stability than SiC in air [1–3]. Intermetallic NiAl particles can be considered as a potential

reinforcement to fabricate ceramic matrix composites for high-temperature applications, because they possess high specific strength, high thermal stability, good oxidation resistance, high elastic modulus, a high melting temperature of about 1640 °C, and a similar coefficient of thermal expansion to Al_2O_3 [3,7,8]. It is expected that the incorporation of NiAl particles in Al_2O_3 matrixes could lessen structural deficiencies resulting from incompatibility between metallic reinforcements and ceramic matrix and thereby improve interfacial stability between them for the reliability, durability, and service life of Al_2O_3MCs [7–9].

Nowadays, the SPS technology has been widely used in powder industries because of its capability to produce nanostructured materials with relatively lower porosity densities compared to that of the conventional sintering (CS) technology [10]. SPS materials usually possess higher hardness and wear resistance than CS ones [11]. It is expected that SPS Al_2O_3MCs reinforced with NiAl particles could be potentially applied to gas turbine components. Huang et al. [7] used the SPS technology to develop NiAl particle-reinforced Al_2O_3MCs, which had an 80% increase in fracture toughness at the NiAl particle content of 15 wt.%. Beyhaghi et al. [12] developed SPS NiAl-Al_2O_3MC coatings from Ni, NiO, and Al powder on cast iron and investigated their mechanical properties. In the study of Zygmuntowicz et al. [13], the hardness and frictional behavior of pulse plasma-sintered Al_2O_3MCs from a mixture of Al_2O_3 and NiAl-Al_2O_3 were investigated with different sintering temperatures, but their friction remained relatively high. It has been noticed that most of the reports in the literature are related to the microstructures and mechanical properties of NiAl particle-reinforced Al_2O_3MCs, but very few reports on their tribological properties are found, mostly with one or two compositions. Designing starting power materials is relatively important to produce end products with desired properties, which is still limited for a better understanding. Therefore, a comprehensive study is necessary to understand the effects of NiAl particle content on the mechanical and tribological properties of SPS Al_2O_3MCs for their successful adaptation in gas turbine components.

In this study, the Al_2O_3MCs with different NiAl particle contents of 5–20 wt.% were fabricated via SPS processes. The maximum NiAl particle content was optimized not to exceed more than 20 wt.%, based on the previous research reported in [7], as well as in order to maintain their reasonably high performance, since the high metal content could dramatically degrade their mechanical strength and tribological performance, especially at high working temperatures. The field emission scanning electron microscopy (FESEM) was used to observe the microstructures of the Al_2O_3MCs, as their fracture and hardness were evaluated with Vickers hardness tests. A ball-on-disc micro-tribological test was applied to investigate the friction and wear of the Al_2O_3MCs during rubbing contact with 6 mm Al_2O_3 balls under 2 and 6 N loads at a laboratory room temperature (LRT) of 22–24 °C.

2. Materials and Methods

2.1. Sample Preparation

The starting materials were commercially available Al_2O_3 particles (MR70, 99.8%, Martinswerk, Bergheim, Germany) and NiAl particles (Al-Ni-01-P.20UM, American Element, Los Angeles, CA, USA). The average sizes of the as-received Al_2O_3 and NiAl particles were 0.65 and 10 μm, respectively. The as-received NiAl particles were milled in a planetary stainless-steel container with stainless balls and an ethanol solution for 5 h to achieve an average particle size of 1 μm. Then the milled NiAl particles were dried in an oven at a temperature of 80 °C for 24 h, which completely evaporated the remaining ethanol.

The Dr. Sinter 1050 SPS system was used to fabricate the Al_2O_3 and Al_2O_3MCs with 5, 10, 15, and 20 wt.% NiAl particles. The mixture of Al_2O_3 and NiAl particles with a total weight of 1 g was loaded into a cylindrical graphite die that had a hollow with a diameter of 10 mm for each batch. The die was automatically heated up to 600 °C in the first 3 min,

then to 1300 °C at a heating rate of 100 °C/min, held for 3 min under a sintering pressure of 50 MPa, and cooled down to the LRT at a cooling rate of 100 °C/min. The sintering temperature was monitored with an infrared thermometer focused on the die wall. The same SPS process was applied for the pure NiAl specimen, except for using a lower peak sintering temperature of about 1000 °C. Two to three specimens for each NiAl particle content were prepared. The thickness of the SPS samples was about 5 mm.

2.2. Characterization

The surface chemical structures of the SPS samples were examined using X-ray photoelectron spectroscopic measurements (XPS) on a Kratos Axis-ULTRA, Manchester, UK. An Al Kα monochromatic X-ray of 1486.6 eV was used.

The microstructures, indentation-induced microcracks, and worn surfaces of the SPS samples were observed by FESEM (JEOL JSM-7600F, Tokyo, Japan) and optical (Zeiss Axioskop 2, JVC color video camera, Wetzlar, Germany) micrographs. The energy-dispersive X-ray spectroscopy (EDX) built into the FESEM was applied to measure the chemical compositions of their wear tracks. The EDX analysis was performed at points. A thin gold layer was applied on their surfaces to avoid a charging effect during the FESEM measurements.

The Talyscan 150 surface profilometry (Taylor Hobson LTD, Leicester, UK) was applied to scan the 3D wear tracks of the SPS samples in a scan area of 0.5 mm × 0.3 mm. A contact mode diamond stylus with a diameter of 4 μm was used.

The hardness values of the SPS samples were measured with Vickers hardness tests (Future-tech FM-300e, Kawasaki, Japan) under a 19.6 N load with a holding time of 5 s at the peak load. Indentations were carried out at five randomly selected places on each sample surface to take their average hardness.

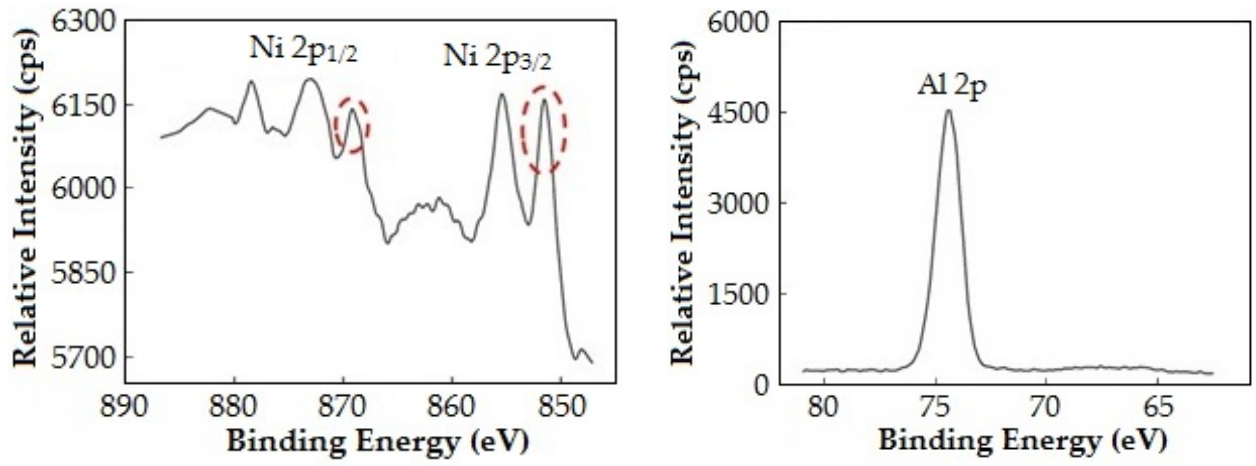
The friction of the SPS samples was measured using a ball-on-disc micro-tribological test (CSM Instrument, Peseux, Switzerland) (DIN50324 and ASTM G99). Their surface wear was generated by rotating them against a fixed Al_2O_3 ball with a diameter of 6 mm in a 2 mm circular path for 80,000 laps at a sliding speed of 2 cm/s under 2 and 6 N loads at the LRT. Three to five measurements for each sample were executed to get an average friction coefficient. Their wear widths and depths were measured using surface profilometry to further calculate their specific wear rates (k), according to the following equation [14]:

$$k = V/(F \times s)$$

where V, F, and s are denoted as the wear volume, normal load, and total sliding distance, respectively.

3. Results and Discussion

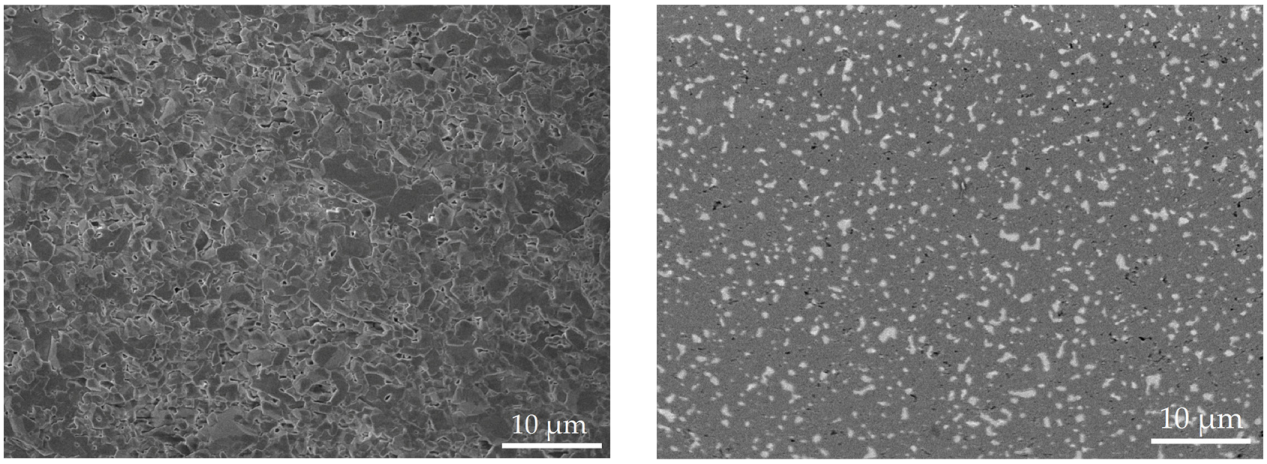
The XPS Ni 2p and Al 2p peaks of the Al_2O_3MC with 20 wt.% NiAl particles are illustrated in Figure 1. The Ni $2p_{3/2}$ and Ni $2p_{1/2}$ peaks at about 856 eV and 873 eV and their associated satellite peaks at about 862 eV and 878 eV, respectively, are found in Figure 1a, which are attributed to Ni in the form of oxides [7,15]. The additional two peaks at about 852 eV and 868 eV, as indicated by the circles in Figure 1a, come from metallic Ni in NiAl [7,16]. The Al 2p peak at about 74.5 eV (Figure 1b) is attributed to Al in Al_2O_3 [7,17].



(**a**) (**b**)

Figure 1. XPS (**a**) Ni 2p and (**b**) Al 2p peaks of Al_2O_3MC with 20 wt.% NiAl particles.

The Al_2O_3 possesses a microstructure with micrograins and micropores, as shown in Figure 2a. However, the microstructure of the Al_2O_3MC with 20 wt.% NiAl particles (Figure 2b) is apparently different from that of the Al_2O_3 due to the lack of micrograins and the uniform distribution of white NiAl particles in its microstructure. Nanopores still exist in its microstructure, indicating that the development of the SPS Al_2O_3MCs with NiAl particles effectively suppresses micrograins and micropores in their microstructures [7,18].



(**a**) (**b**)

Figure 2. Microstructures of (**a**) Al_2O_3 and (**b**) Al_2O_3MC with 20 wt.% NiAl particles.

The indents on the surfaces of the Al_2O_3 and Al_2O_3MC with 20 wt.% NiAl particles made under a 19.6 N load can be compared in Figure 3a,b. The Al_2O_3MC has less indentation-induced microcracking than the Al_2O_3, because the lack of grain boundaries and micropores in its microstructure results in its reduced brittleness and, thereby, its improved fracture resistance [7,19,20].

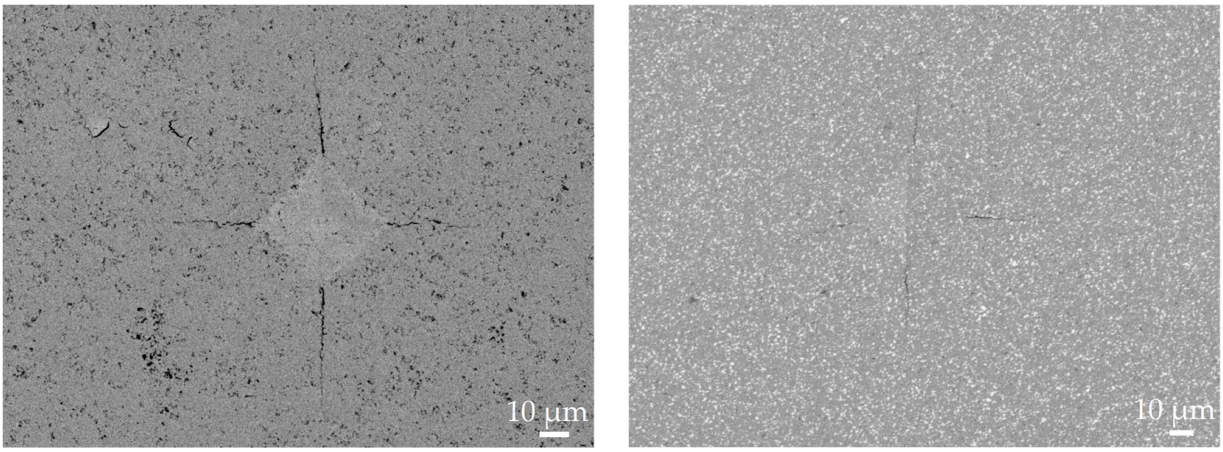


Figure 3. Indents on surfaces of (**a**) Al_2O_3 and (**b**) Al_2O_3MC with 20 wt.% NiAl particles made under a 19.6 N load.

The hardness of the Al_2O_3 is 2102 Hv (Figure 4). The 5 wt.% NiAl particle incorporation reduces the hardness of the Al_2O_3MCs to 1837 Hv (12.6% lower), while the increased NiAl particle content to 20 wt.% further decreases their hardness to 1600 Hv, which is 23.9% and 12.9% lower than those of the ones with 0 and 5 wt.% NiAl particles, respectively. The reason is that the NiAl has a much lower hardness of 733 ± 12 Hv (65.1% lower) than the Al_2O_3 so that the increased NiAl particle content leads to a decrease in the hardness of the Al_2O_3MCs [21,22].

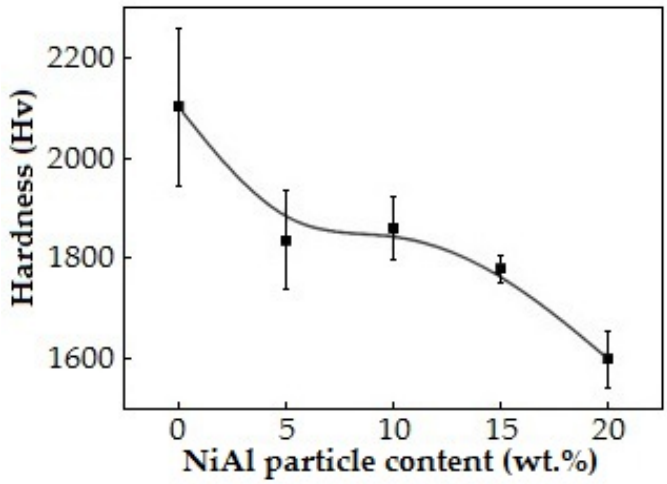
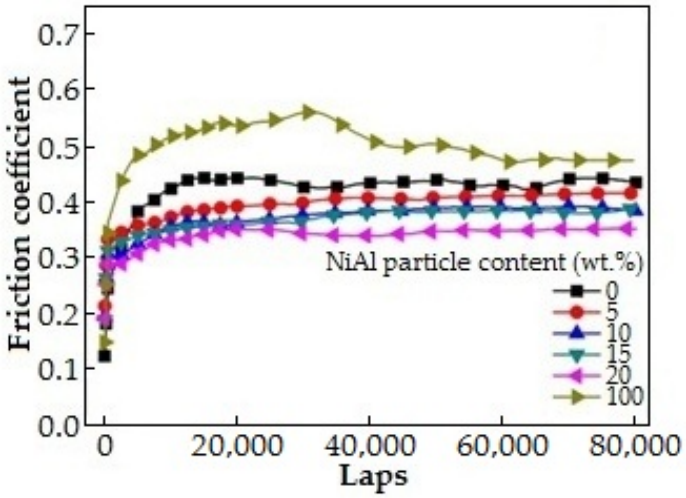
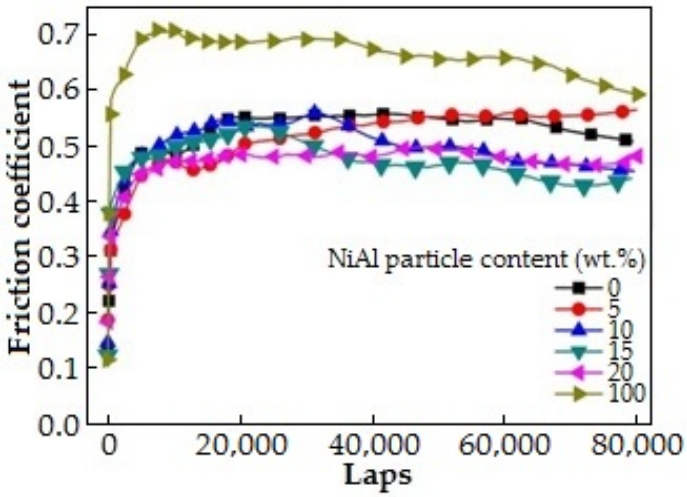


Figure 4. Hardness values of Al_2O_3 and Al_2O_3MCs with different NiAl particle contents.

In Figure 5a,b, the NiAl exhibits higher friction throughout the test than the Al_2O_3 and Al_2O_3MCs under both 2 and 6 N loads, which can be explained by the larger contact between the NiAl and Al_2O_3 ball [14,23–25]. In the long run, the friction of the NiAl decreases with the increased number of laps via its increased wear, since wear debris released through surface wear not only prevents direct contact between two rubbing surfaces but also rolls/slides under a lateral force for lower friction [26–28]. This effect can be more apparently seen with the higher 6 N load, thanks to the higher wear of the NiAl.



(**a**)



(**b**)

Figure 5. Friction coefficients of Al_2O_3, Al_2O_3MCs with different NiAl particle contents, and NiAl tested under (**a**) 2 and (**b**) 6 N loads, as a function of the number of laps.

The incorporation of 5 wt.% NiAl particles lowers the friction of the Al_2O_3MC throughout the wear tests under both 2 and 6 N loads than those of the Al_2O_3, while the Al_2O_3MC has a more depressed trend of friction coefficient versus laps with a higher NiAl particle content. It confirms that the incorporation of NiAl particles or the increased content of NiAl particles decreases the friction of the Al_2O_3MCs during the entire sliding. The comparison of Figure 5a,b confirms that the higher normal load is responsible for the higher friction of the Al_2O_3, Al_2O_3MCs, and NiAl.

In Figure 6, the friction coefficients of the Al_2O_3 under the 2 and 6 N loads are 0.429 and 0.542 (26.3% higher), respectively. The friction coefficients of the NiAl are 0.603 $\pm$ 0.004 for the 2 N load and 0.663 $\pm$ 0.015 (10% higher) for the 6 N load, which are 40.6% and 22.3% higher than those of the Al_2O_3, respectively. It is hypothesized that the contact between dissimilar materials of the NiAl and Al_2O_3 ball is larger via larger deformation and higher wear of the NiAl compared to that between similar materials of the Al_2O_3 and Al_2O_3 ball, which gives rise to the higher friction of the tribopair of the NiAl and Al_2O_3 ball by making more contact junction points between them [14,23–25].

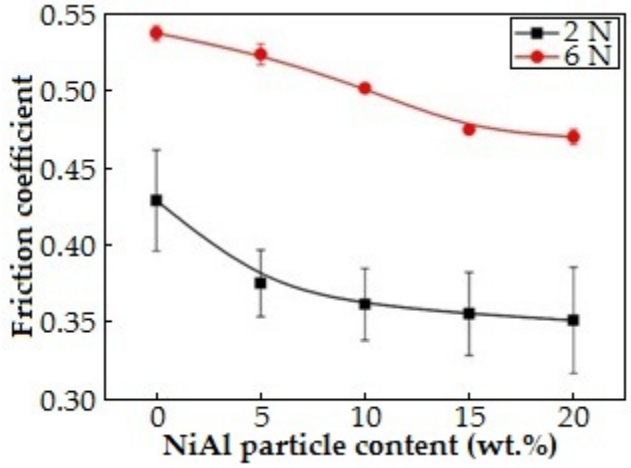


Figure 6. Friction coefficients of Al_2O_3 and Al_2O_3MCs with different NiAl particle contents tested under 2 and 6 N loads.

The friction coefficients of the Al_2O_3MCs decrease from 0.375 to 0.351 (6.4% lower) for the 2 N load and from 0.523 to 0.470 (10.1% lower) for the 6 N load with an increased NiAl particle content from 5 to 20 wt.%. The Al_2O_3MC with 20 wt.% NiAl particles has 18.2% and 13.3% lower friction coefficients under the 2 and 6 N loads, respectively, than the Al_2O_3. Although the friction of the NiAl is apparently higher compared to that of the Al_2O_3, the friction coefficients of the Al_2O_3MCs under both 2 and 6 N loads do not increase with the increased content of NiAl particles. It indicates that the metallic friction of the NiAl does not apparently contribute to that of the Al_2O_3MCs in this study. Normally, high interfacial shear strength between two contacting surfaces causes high friction during dry sliding [29–32]. Since intimate contact between the very hard Al_2O_3 and Al_2O_3 ball generates high friction by causing high contact pressure and interfacial shear strength between them, especially at contact junction points, under the applied normal load, it is hypothesized that the incorporation of NiAl particles with much lower hardness decreases the interfacial shear strength between the rubbing Al_2O_3 surfaces via plastic deformation and flow of the particles at intimate contact points in the dry sliding process. In addition, rigid mechanical interlocking between mating asperities of the rubbing Al_2O_3 surfaces gives rise to high friction, so the existence of NiAl particles on one of the rubbing surfaces replaces hard ceramic asperities with much softer metallic ones to make them easier to slide over each other [7,33–35]. As a result, the increased NiAl particle content in Al_2O_3 matrixes leads to the decreased friction of the Al_2O_3MCs by decreasing the interfacial shear strength.

The friction coefficients of the NiAl, Al_2O_3, and Al_2O_3MCs are obviously higher under the higher 6 N load (Figure 6). Their higher surface wear associated with the higher normal load should be taken into account, resulting in their larger contact with their counter Al_2O_3 balls and, thereby, a larger number of contact junction points between the rubbing surfaces for the higher interfacial shear strength [14,23–25].

The specific wear rates of the Al_2O_3 under the 2 and 6 N loads are 352.9 $\times$ 10^{-18} and 1027.7 $\times$ 10^{-18} m^3/(Nm) (191.2% higher), respectively, as found in Figure 7. The specific wear rates of the NiAl are 1986.7 $\pm$ 891.2 $\times$ 10^{-18} m^3/(Nm) for the 2 N load and 6410.8 $\pm$ 1786.9 $\times$ 10^{-18} m^3/(Nm) for the 6 N load (222.7% higher), which are 463% and 523.8% higher than those of the Al_2O_3, respectively. This indicates that the NiAl has lower wear resistance than the Al_2O_3, as they both have higher wear associated with the higher normal load [36,37].

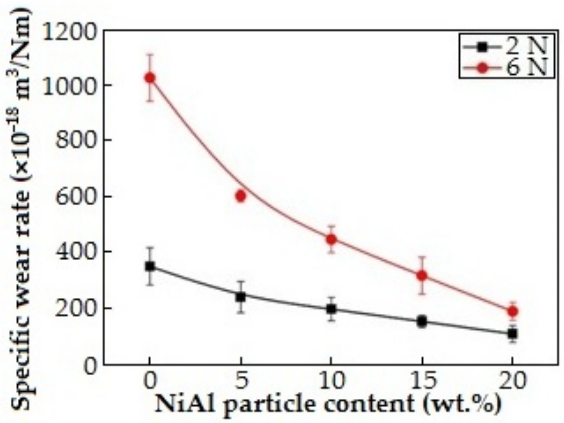


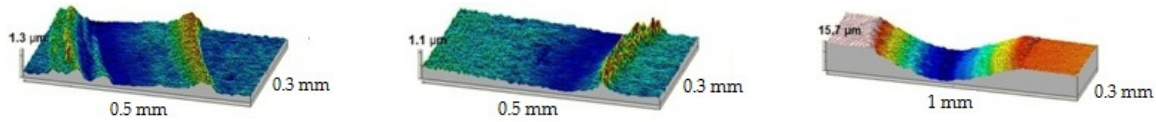
Figure 7. Specific wear rates of Al_2O_3 and Al_2O_3MCs with different NiAl particle contents tested under 2 and 6 N loads.

Under the 2 N load, the specific wear rate of the Al_2O_3MC with 5 wt.% NiAl particles is 243 × 10^{-18} m^3/(Nm), which is 31.14% lower than that of the Al_2O_3, as increasing the NiAl particle content to 20 wt.% results in the further decreased specific wear rate of the Al_2O_3MC to 111.8 × 10^{-18} m^3/(Nm), which is 68.3% and 54% lower than those of the Al_2O_3 and Al_2O_3MC with 5 wt.% NiAl particles, respectively. Under the 6 N load, the increased NiAl content from 5 to 20 wt.% also decreases the specific wear rates of the Al_2O_3MC from 606 × 10^{-18} to 192 × 10^{-18} m^3/(Nm) (68.3% lower). The specific wear of the Al_2O_3MC with 20 wt.% NiAl particles is 71.7% higher for the higher 6 N load but 81.3% lower than the Al_2O_3 for the same 6 N load.

Generally, the surface abrasive wear of the Al_2O_3MCs results from the dry sliding of their Al_2O_3 balls [29,36,37]. Therefore, the decreased friction of the Al_2O_3MCs with an increased NiAl particle content leads to their lowered abrasive wear. It is known that solid materials with higher surface hardness have higher abrasive wear resistance under dry conditions [14,38,39]. However, there is not a proper correlation between the hardness (Figure 4) and wear (Figure 7) of the Al_2O_3MCs with different NiAl particle contents, implying that their reduced friction with the NiAl particle incorporation lessens the influence of their hardness on their abrasive wear during the dry sliding.

Fatigue wear can also be considered a major contributor to the wear of the low fracture-resistant Al_2O_3 [29,36,37,39]. The repeated dry sliding of the Al_2O_3 ball results in the initiation of minute fatigue cracks in a subsurface region, especially at microstructural defects, such as micrograins and micropores, and their substantial propagation parallel to a free surface through the defects before surface materials are removed as micro-platelets [36,37,39–41]. The continuous development of such surface material spallation leads to fatigue wear [36,37,39–41]. Therefore, the wear of the Al_2O_3 possessing such micrograins and micropores is greatly attributed to the fatigue wear. As found in Figure 2b, the incorporation of NiAl particles suppresses the micrograins and micropores of the Al_2O_3MCs, which in turn effectively prevents the initiation and propagation of fatigue cracks and thereby their fatigue wear during the repeated dry sliding. Furthermore, the 3D distribution of NiAl particles in their matrixes also greatly lessens their fatigue wear by stopping the further propagation of fatigue cracks. As a result, the fatigue wear of the Al_2O_3MCs further decreases with their increased NiAl particle content [36,37,39–41]. Since the higher normal load gives rise to not only the more severe abrasive wear by exerting a larger normal force on the counter Al_2O_3 ball but also the higher fatigue wear via a larger amplitude of cyclic loading [14,42,43], the higher wear of the Al_2O_3 and Al_2O_3MCs is found under the higher 6 N load, as reported in Figure 7.

An apparent wear track is found on the surface of the Al_2O_3 tested under the 6 N load in addition to a pile of materials along both sides of its wear track, as shown in Figure 8a, because the repeated dry sliding of the Al_2O_3 ball pushes surface materials to both sides of the wear track by initiating minute cracks in the subsurface region and propagating them parallel to the surface [36,37,39–41]. This is indicative of the fatigue wear of the Al_2O_3. In Figure 8b, the Al_2O_3MC with 20 wt.% NiAl particles has a smaller wear track with less piling of surface materials on the sides as a result of its improved fracture resistance. The wear track of the NiAl (Figure 8c) is apparently larger than those of the Al_2O_3 (Figure 8a) and Al_2O_3MC with 20 wt.% NiAl particles (Figure 8b) under the same 6 N load, blaming its lower wear resistance for it. No observation of a pile of surface materials on the wear track of the NiAl indicates the dominance of its abrasive wear.



(**a**) (**b**) (**c**)

Figure 8. Wear topographies of (**a**) Al_2O_3, (**b**) Al_2O_3MC with 20 wt.% NiAl particles, and (**c**) NiAl tested under a 6 N load.

A larger wear track with more apparent abrasive lines is found on the wear morphology of the NiAl tested under the higher 6 N load, as shown by the comparison of Figure 9a,b [14,38,39]. Furthermore, microcracks are found on its wear track only under the higher 6 N load (Figure 9d) as a result of the larger amplitude of cyclic loading [42,43], indicating that it is more susceptible to fatigue cracking under the higher normal load. The formation of tribolayers on its wear tracks is observed for both 2 and 6 N loads [14,44–46].

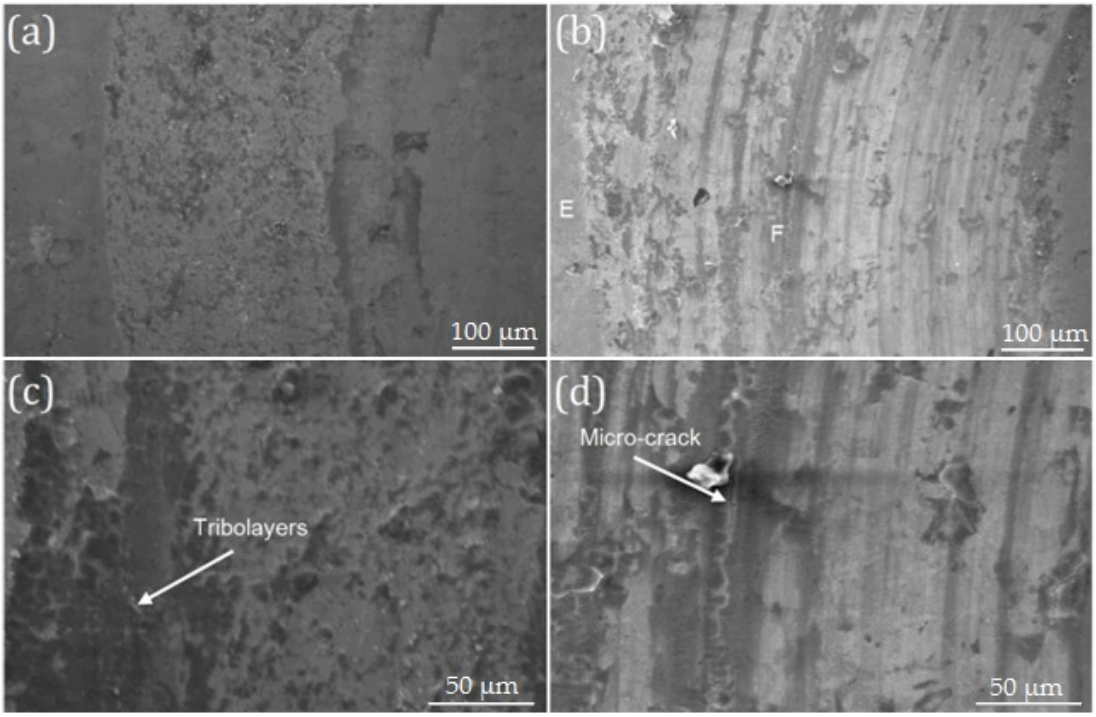


Figure 9. Wear morphologies of NiAl, tested under (**a**,**c**) 2 and (**b**,**d**) 6 N loads, observed at different magnifications.

In the wear morphologies of Figure 10a–d, the Al_2O_3MC with 20 wt.% NiAl particles has smaller wear tracks than the Al_2O_3 under both 2 and 6 N loads, as they both have

larger wear tracks under the higher 6 N load. The Al_2O_3 (Figure 10a,c) has piles of surface materials on the circumferences of its wear tracks under both 2 and 6 N loads. But such material piling is not apparent for the Al_2O_3MC with 20 wt.% NiAl particles, especially for the 2 N load (Figure 10b), because its improved fracture resistance lessens the material piling by preventing the initiation and propagation of fatigue microcracks in the sliding process.

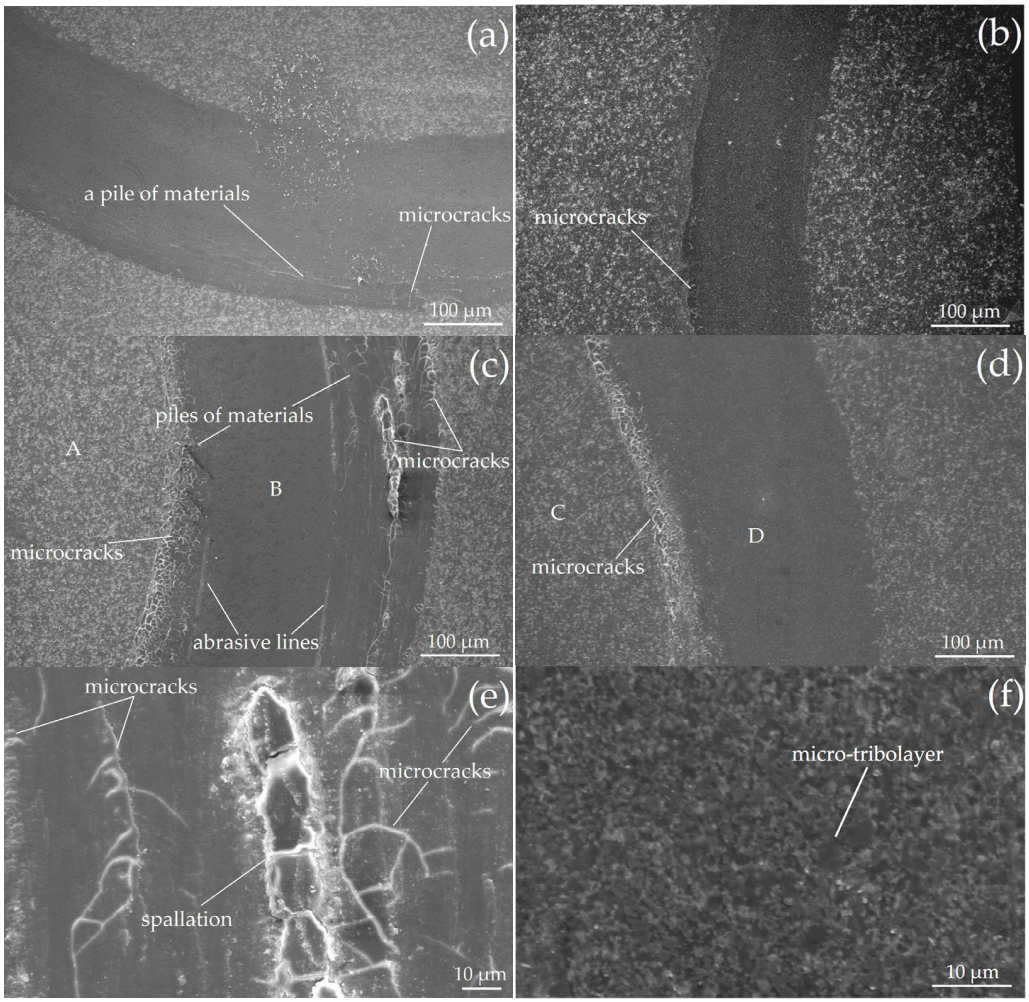


Figure 10. Wear morphologies of (**a**,**c**,**e**) Al_2O_3 and (**b**,**d**,**f**) Al_2O_3MC with 20 wt.% NiAl particles tested under (**a**,**b**) 2 and (**c**–**f**) 6 N loads.

Under the higher 6 N load, both the Al_2O_3 and Al_2O_3MC with 20 wt.% NiAl particles exhibit more apparent piling of surface materials on their wear tracks via more severe fatigue cracking, so fatigue microcracks and micro-platelets are more apparently found on their wear tracks (Figure 10c,d) [42,43]. Some abrasive lines composed of microcracks and micro-platelets are found on the wear track of the Al_2O_3 but not on the wear track of the Al_2O_3MC with 20 wt.% NiAl particles under the higher 6 N load (Figure 10c). This confirms that the Al_2O_3MCs are less susceptible to fatigue wear than the Al_2O_3,thanks to their improved fracture resistance [36,37,39–41].

In Figure 10e, microcracks on the wear track of the Al_2O_3 tested under the 6 N load are obvious with the removal of surface materials as micro-platelets [33,34,36–38]. The networking of microcracks initiated and propagated parallel or/and perpendicular to the sliding direction is also found on its wear track. Such microcracks are not apparently found on the wear track of the Al_2O_3MC with 20 wt.% NiAl particles under the same 6 N load, as shown in Figure 10f.

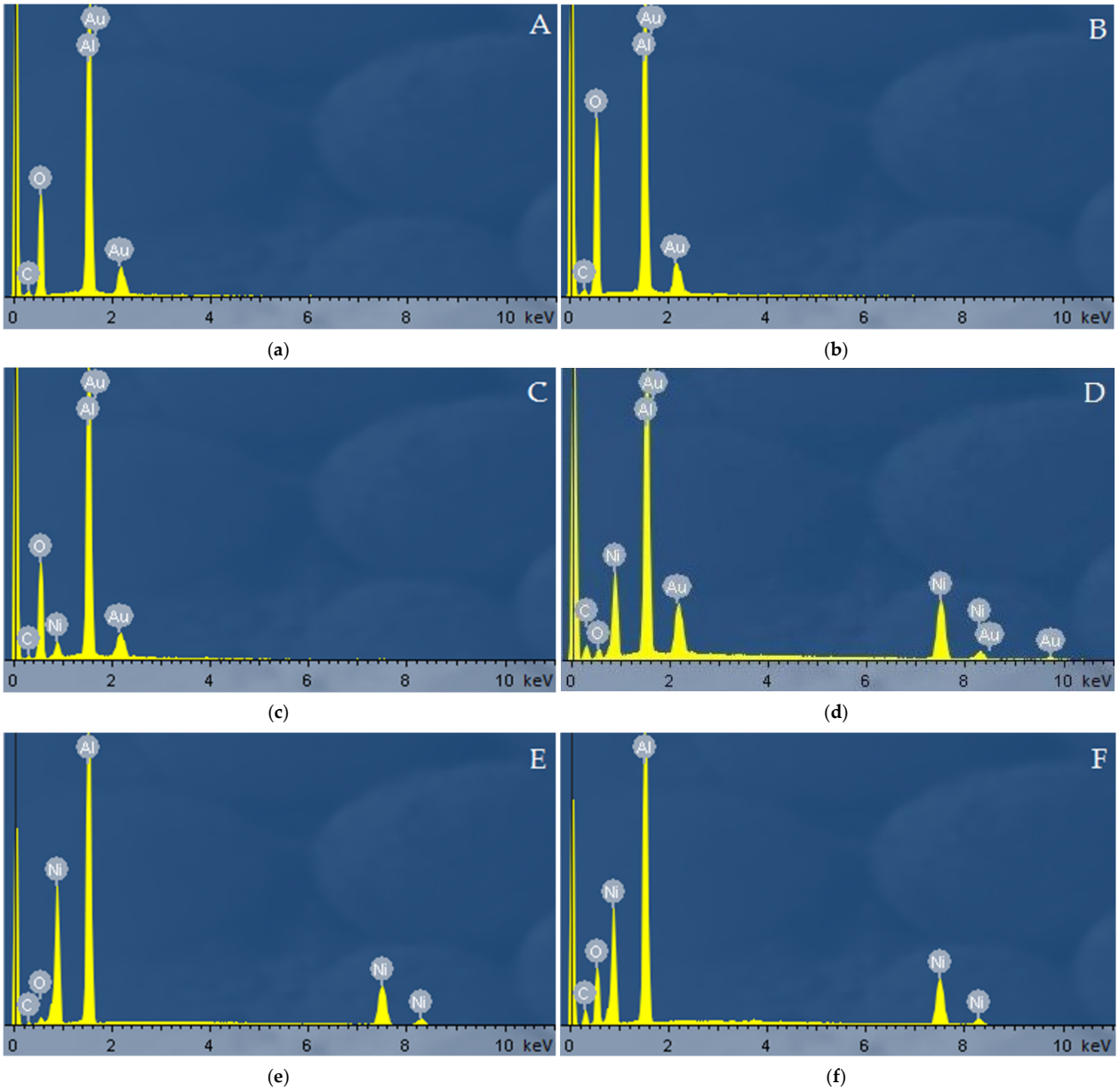
Micro-tribolayers are found on the wear track of the Al_2O_3MC with 20 wt.% NiAl particles at a higher magnification in Figure 10f. Generally, very hard Al_2O_3 wear debris cannot be easily deformed and compacted so that the Al_2O_3 wear debris serves as abrasive particles for three-body abrasive wear [44]. It is supposed that the release of embedded NiAl particles via surface wear makes them much easier to be deformed and compacted to form the micro-tribolayers during the repeated dry sliding [45,46]. The micro-tribolayers serve as micro-slipping-layers and micro-spacers at intimate contact points between two rubbing surfaces to effectively reduce the interfacial shear strength [14,45,46]. Therefore, the formation of micro-tribolayers is one of the reasons to effectively reduce the friction and wear of the Al_2O_3MCs.

The roughened surface of the Al_2O_3 associated with its fatigue wear causes strong mechanical interlocking between the rubbing Al_2O_3 surfaces to generate high friction during the dry sliding [7,30–32]. Therefore, the reduced surface wear of the Al_2O_3MC with the incorporation of NiAl particles can also be related to its lower friction as a consequence of its lessened surface roughening.

Both the EDX spectra of the Al_2O_3 measured on its untested area and wear track have C, Al, O, and Au peaks, as found in Figure 11a,b. The C peak is indicative of surface carbon contaminants, while the Al and O peaks are attributed to the Al_2O_3 matrix [14,47,48]. The Au peak comes from the surface gold layer of the Al_2O_3. The Al_2O_3 has a stronger EDX O peak for its wear track (Figure 11b) than for its untested area (Figure 11a) due to the occurrence of friction-induced oxidation in the dry sliding process [14,45,46]. Both the EDX spectra of the Al_2O_3MC with 20 wt.% NiAl particles measured on its untested area (Figure 11c) and wear track (Figure 11d) have an additional Ni peak that is attributed to the embedded NiAl particles. In the comparison of Figure 11c,d, the EDX spectrum of the Al_2O_3MC has a stronger Ni peak and a weaker O peak for its wear track than for its untested area. The reason is that the existence of micro-tribolayers mainly composed of NiAl wear debris on its wear track (Figure 10f) gives rise to the stronger Ni peak as well as the weaker O peak. The Al_2O_3MC (Figure 11d) has the weaker O peak on the EDX spectra of the wear track than the Al_2O_3 (Figure 11b), because its lowered friction with the incorporation of NiAl particles hinders the friction-induced oxidation process.

The C, Ni, Al, and O peaks are found on both the EDX spectra of the NiAl measured on its untested area (Figure 11e) and wear track (Figure 11f). The NiAl matrix contributes to the Ni and Al peaks, as surface carbon and oxygen contaminants are responsible for the C and O peaks, respectively [14,47,48]. The stronger O peak on the EDX spectrum of its wear track is the result of the friction-induced oxidation [14,45,46].

The surfaces of the counter Al_2O_3 balls slid on the Al_2O_3, Al_2O_3MC with 20 wt.% NiAl particles, and NiAl under the 6 N load were examined after the tribo-tests. In Figure 12a, the Al_2O_3 ball rubbed on the Al_2O_3had an apparent wear scar with abrasive lines. Such abrasive lines result from the roughened surface of the Al_2O_3 associated with its fatigue wear, because its roughened surface serves as an abrading surface to abrade its counter-ball surface [32]. Fatigue cracking of the Al_2O_3 ball is not found in Figure 12a. The wear scar of the Al_2O_3 ball tested on the Al_2O_3MC with 20 wt.% NiAl particles (Figure 12b) is much smaller than that of the one rubbed on the Al_2O_3 (Figure 12a), which implies that the incorporation of NiAl particles apparently decreases the abrasive wear of both the Al_2O_3MC and Al_2O_3 ball by reducing their friction. Transferred materials (black spots) are found on the wear scar of the Al_2O_3 ball rotated on the Al_2O_3MC (Figure 12b) but not on that of the one rubbed on the Al_2O_3 (Figure 12a). In Figure 12c, the Al_2O_3 ball rubbed on the NiAl does not have any abrasive wear scar but has the largest amount of transferred materials, which are identified as NiAl materials, because the Al_2O_3 ball has much higher abrasive wear resistance than the NiAl.

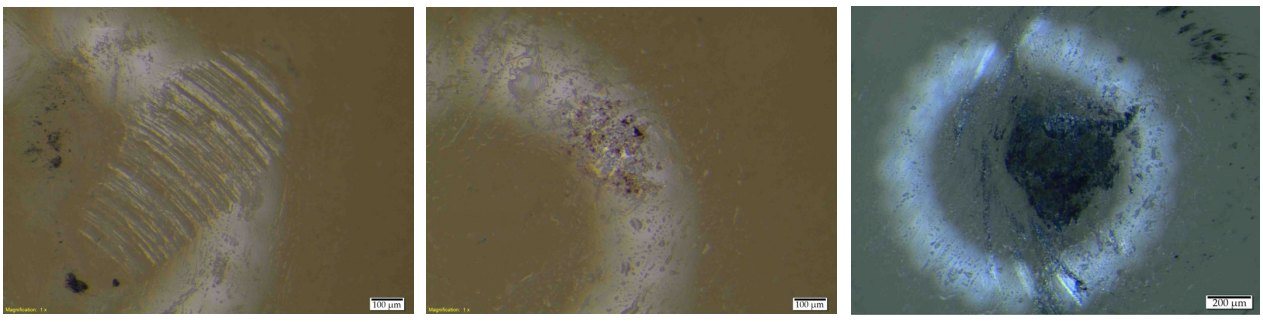


(**a**) (**b**)

(**c**) (**d**)

(**e**) (**f**)

Figure 11. EDX spectra of (**a**,**b**) Al_2O_3, (**c**,**d**) Al_2O_3MC with 20 wt.% NiAl particles, and (**e**,**f**) NiAl tested under a 6 N load, measured at locations (**a**) 'A' in untested area and (**b**) 'B' in wear track of Figure 10c, (**c**) 'C' in untested area and (**d**) 'D' in wear track of Figure 10d, and (**e**) 'E' in untested area and (**f**) 'F' in wear track of Figure 9b.



(**a**) (**b**) (**c**)

Figure 12. Wear morphologies of Al_2O_3 balls slid on (**a**) Al_2O_3, (**b**) Al_2O_3MC with 20 wt.% NiAl particles, and (**c**) NiAl tested under a6 N load. The scale bars of 100 μm, 100 μm, and 200 μm are used in (**a**–**c**), respectively.

4. Conclusions

The SPS technology was used to develop the Al_2O_3MCs with different NiAl particle contents to study their microstructures, fracture, hardness, friction, and wear.

- The Al_2O_3 possessed a microstructure with micrograins and micropores, but the Al_2O_3MCs did not. As a result, the Al_2O_3MCs exhibited higher fracture resistance than the Al_2O_3 in the indentation-induced crack tests.
- The much lower hardness of NiAl particles compared to that of the Al_2O_3 matrix led to the decreased hardness of the Al_2O_3MCs with an increased NiAl particle content so that the Al_2O_3MC with 20 wt.% NiAl particle content had 23.9% lower hardness than the Al_2O_3.
- The increased NiAl particle content decreased the friction of the Al_2O_3MCs under both 2 and 6 N loads as a result of the lubricating effect of embedded NiAl particles. Therefore, the Al_2O_3MC with 20 wt.% NiAl particle content had 18.2% and 13.3% lower friction than the Al_2O_3 for the 2 and 6 N loads, respectively.
- The Al_2O_3MCs had an apparent decrease in their wear with an increased NiAl particle content under both 2 and 6 N loads due to their decreased abrasive and fatigue wear associated with their reduced friction and improved fracture resistance, respectively. The Al_2O_3MC with 20 wt.% NiAl particle content had 68.3% and 81.3% lower wear than the Al_2O_3 under the 2 and 6 N loads, respectively.
- Under the higher 6 N load, both the Al_2O_3 and Al_2O_3MCs exhibited higher friction and wear, as they both were more susceptible to fatigue cracking. Nevertheless, the Al_2O_3MCs had better tribological performance than the Al_2O_3.
- It could be concluded that the incorporation of NiAl particles lowered the hardness but improved the fracture and wear resistance of the Al_2O_3MCs.
- The SPS Al_2O_3MCs with NiAl particles have relatively low friction and wear, which would be beneficial for rotating gas turbine components.

Author Contributions: Conceptualization, methodology, validation, formal analysis, investigation, data curation, writing—original draft preparation, writing—review and editing, and visualization, N.W.K.; sample preparation, M.H., H.Z. and Z.A.L.; supervision, J.Y., K.A.K. and F.D. All authors have read and agreed to the published version of the manuscript.

Funding: The authors acknowledge the financial support from Singapore DSO National Laboratories (project agreement no.: DSOCL10303).

Data Availability Statement: The raw data supporting the conclusions of this article will be made available by the authors upon request.

Conflicts of Interest: The authors declare no conflicts of interest.

References

1. Mark, V.R. Ceramic gas turbine development: Need for a 10-year plan. *J. Eng. Gas Turbines Power* **2010**, *131*, 011301.
2. Easley, M.L.; Symth, J.R. Ceramic gas turbine technology development. *J. Eng. Gas Turbines Power* **1995**, *117*, 783–791. [CrossRef]
3. Oskarsson, H. Material challenges in industrial gas turbines. *J. Iron Steel Res. Int.* **2007**, *14*, 11–14. [CrossRef]
4. Bhattacharya, S.; Singh, I.V.; Misha, B.K. Fatigue life simulation of functionally graded materials under cyclic thermal loading using XFEM. *Int. J. Mech. Sci.* **2014**, *82*, 41–59. [CrossRef]
5. Atïk, E. Mechanical properties and wear strengths in aluminum-alumina composites. *Mater. Struct.* **1998**, *31*, 418–422. [CrossRef]
6. Kenis, P.J.A. Fabrication of ceramic microscale structures. *J. Am. Ceram. Soc.* **2007**, *90*, 2779–2783.
7. Huang, M.; Zhong, L.; Jin, W.; Khor, K.A.; Huo, F.W.; Duan, F.; Lim, S.C.; Yip, M.S.; Yang, J.L. Multifunctional alumina composites with toughening and crack-healing features via incorporation of NiAl particles. *J. Am. Ceram. Soc.* **2015**, *98*, 1618–1625. [CrossRef]
8. Chmielewski, M.; Nosewicz, S.; Pietrzak, K.; Rojek, J.; Nedza, A.S.; Mackiewics, S.; Dutkiewicz, J. Sintering behaviour and mechanical properties of NiAl, Al_2O_3 and NiAl-Al_2O_3 composites. *J. Mater. Eng. Perform.* **2014**, *23*, 3875–3886. [CrossRef]

9. Abe, O.; Takata, S.; Ohwa, Y. Toughening of NiAl-alumina composites by self-constructed compressive surface layers under oxidation. *J. Eur. Ceram. Soc.* **2004**, *24*, 489–494. [CrossRef]
10. Tokita, M. Progress of spark plasma sintering method, systems, ceramics applications, and industrialization. *Ceramics* **2021**, *4*, 160–198. [CrossRef]
11. Manohar, G.; Pandey, K.M.; Maity, S.R. Effect of spark plasma sintering on microstructure and mechanical properties of AA7075/B_4C/ZrC hybrid nanocomposites fabricated by powder metallurgy techniques. *Mater. Chem. Phys.* **2022**, *282*, 126000. [CrossRef]
12. Beyhaghi, M.; Rashid, A.R.K.; Kashefi, M.; Khaki, J.V.; Jonsson, S. Effect of powder reactivity on fabrication and properties of NiAl/Al2O3 composite coated on cast iron using spark plasma sintering. *Appl. Surf. Sci.* **2015**, *344*, 1–8. [CrossRef]
13. Zygmuntowicz, J.; Konopka, K.; Krannowski, M.; Piotrkiewicz, P.; Wachowski, M.; Zurowski, R.; Cymerman, K.; Kulikowski, K.; Sobiecki, R. Microstructure and mechanical characterization of novel Al2O3-(NiAl-Al2O3) composites fabricated via pulse plasma sintering. *Materials* **2023**, *16*, 4316. [CrossRef] [PubMed]
14. Khun, N.W.; Toh, W.Q.; Liu, E. Study on changes in hardness and wear resistance of 3D printed Ti-6Al4-V with respect to heat treatment temperature. *Tribol. Ind.* **2023**, *45*, 129–135. [CrossRef]
15. Ohtsu, N.; Oku, M.; Obara, K.; Ito, S.; Shisido, T.; Wagatsuma, K. Oxidation behavior of NiAl alloy at low temperatures. *Surf. Interface Anal.* **2007**, *39*, 528–532. [CrossRef]
16. Parola, V.L.; Pantaleo, G.; Liotta, L.F.; Venezia, A.M.; Gabrovska, M.; Nikolova, D.; Tabakova, T. Gold and ceria modified NiAl hydrotalcite materials as catalyst precursors for dry reforming of methane. *Catalysts* **2023**, *13*, 606. [CrossRef]
17. Snijiders, P.C.; Jeurgens, L.P.H.; Sloof, W.G. Structure of thin aluminum-oxide films determined from valence band spectra measured using XPS. *Surf. Sci.* **2002**, *496*, 97–109. [CrossRef]
18. Wang, H.M.; Su, W.X.; Liu, J.Q.; Li, G.R.; Liu, Y.J.; Zhou, P.J. Microstructure and properties of FeCoNiCrMn and Al_2O_3 hybrid particle-reinforced alumina matrix composites fabricated by microwave sintering. *J. Mater. Res. Technol.* **2023**, *24*, 8618–8634. [CrossRef]
19. Larson, D.R.; Coppala, J.A.; Hasselman, D.P.H.; Bradt, R.C. Fracture toughness and spalling behaviour of high Al_2O_3 refractories. *J. Am. Ceram. Soc.* **1974**, *57*, 417–421. [CrossRef]
20. Kim, B.N.; Kishi, T. Estimation of fracture resistance of Al_2O_3 polycrystals from single crystal values. *Mater. Sci. Eng. A* **1994**, *176*, 371–378. [CrossRef]
21. Park, B.G.; Crosky, A.G.; Hellier, A.K. Material characterization and mechanical properties of Al_2O_3-Al metal matrix composites. *J. Mater. Sci.* **2001**, *36*, 2417–2426. [CrossRef]
22. Chakraborty, A.; Kamat, S.V.; Mitra, R.; Ray, K.K. Effect of $MoSi_2$ and Nb reinforcements on mechanical properties of Al_2O_3 matrix composites. *J. Mater. Sci.* **2000**, *35*, 3827–3835. [CrossRef]
23. Tabor, D. Friction: The present state of our understanding. *J. Tribol.* **1981**, *103*, 169–179. [CrossRef]
24. Yao, J.; Wu, Y.; Sun, J.; Tian, J.; Zhou, P.; Bao, Z.; Xia, Z.; Gao, L. Friction and wear characteristics of silicon nitride ceramics under dry friction condition. *Mater. Res. Express* **2021**, *8*, 035701. [CrossRef]
25. Bay, N.; Wanheim, T. Real area of contact and friction stress at high pressure sliding contact. *Wear* **1976**, *38*, 201–209. [CrossRef]
26. Goyal, R.K.; Yadav, M. Study on wear and friction behaviour of graphite flake filled PTFE composites. *J. Appl. Polym. Sci.* **2013**, *127*, 3186–3191. [CrossRef]
27. Kim, J.H.; Park, J.M.; Park, J.K.; Jeon, K.L. Sliding wear and friction behaviour of zirconium alloy with heat-treated Inconel 718. *Nucl. Eng. Des.* **2014**, *269*, 66–71. [CrossRef]
28. Lucas, M.C.M.; Torrent, F.; Pillon, G.P.; Berger, P.; Lavisse, L. Seeking the oxidation mechanism of debris in the fretting wear of titanium functionalized by surface laser treatments. *Coatings* **2023**, *13*, 110. [CrossRef]
29. He, X.; Liu, Z.; Ripley, L.B.; Swensen, V.L.; Wiesner, K.J.G.; Gulner, B.R.; McAndrews, G.R.; Wieser, R.J.; Borovsky, B.P.; Wang, Q.J.; et al. Empirical relationship between interfacial shear stress and contact pressure in micro and macro-scale friction. *Tribol. Int.* **2021**, *155*, 106780. [CrossRef]
30. Mishra, T.; Rooij, M.D.; Shisode, M.; Hazrati, J.; Schipper, D.J. Characterization of interfacial shear strength and its effect on ploughing behaviour in single asperity sliding. *Wear* **2019**, *436–437*, 203042. [CrossRef]
31. Blau, P.J. *Friction Science and Technology*; Marcel Dekker: New York, NY, USA, 1996.
32. Wang, H.J.; Huang, J.D.; Wang, B.; Zhang, Y.; Wang, J. Study on tribological behaviour of laser surface texturing on silicon nitride ceramic under water lubrication. *Lubricants* **2025**, *13*, 21. [CrossRef]
33. Zhang, H.; Chang, L.; Webster, M.N.; Jackson, A. Effects of friction on the contact and deformation behaviour in sliding asperity contacts. *Tribol. Trans. ASME* **2003**, *46*, 514–521. [CrossRef]
34. Ji, R.; Chen, F.; Ying, R.; Zhang, L. Ceramic-titanium alloys artificial hip joint wear simulation and experimental study. *Coatings* **2023**, *13*, 1321. [CrossRef]
35. Wang, B.; Zhang, W.; Liu, Z. Study of the impact of surface topography on wear resistance. *Coatings* **2024**, *14*, 1128. [CrossRef]

36. Gong, M.; Zhang, H.; Hai, W.; Liu, M.; Chen, Y. Microstructure, mechanical, and tribological properties of SiC-AlN-TiB_2 multiphase ceramics. *Lubricants* **2024**, *12*, 412. [CrossRef]
37. Adam, A.A.; Bakar, H.A.; Amani, U.A.; Paijan, L.H.; Wahab, N.A.; Manmat, M.F.; Ali, M.B.; Herawan, S.G.; Ahmad, Z. Effect of sintering parameters on the mechanical properties and wear performance of alumina inserts. *Lubricants* **2022**, *10*, 325. [CrossRef]
38. Jeong, D.H.; Erb, U.; Aust, K.T.; Palumbo, G. The relationship between hardness and abrasive wear resistance of electrodeposited nanocrystalline Ni-P coatings. *Scr. Mater.* **2003**, *48*, 1067–1072. [CrossRef]
39. Benamor, A.; Benamor, H.; Hadji, Y.; Dey, M.; Chiker, N.; Haddad, A.; Badji, R.; Tricoteaux, A.; Erauw, J.P.; Salhi, M.; et al. Wear and friction characteristics of in situ TiC-reinforced Ti_3SiC_2-Ti_5Si_3 composites against 100Cr6 steel counterpart. *Lubricants* **2024**, *12*, 368. [CrossRef]
40. Dauskardt, R.H. A frictional wear mechanism for fatigue crack growth in grain-bridging ceramics. *Acta Metall. Mater.* **1993**, *41*, 2765–2781. [CrossRef]
41. Ritchie, R.Q. Mechanisms of fatigue crack propagation in ductile and brittle solids. *Int. J. Fract.* **1999**, *100*, 55–83. [CrossRef]
42. Guiu, F.; Reece, M.J.; Vaughan, D.A.J. Cyclic fatigue of ceramics. *J. Mater. Sci.* **1991**, *26*, 3275–3286. [CrossRef]
43. Kruzic, J.J.; Arsecularatne, J.A.; Tanaka, C.B.; Hoffman, M.J.; Cesar, P.F. Recent advances in understanding the fatigue and wear behaviour of dental composites and ceramics. *J. Mech. Behav. Biomed. Mater.* **2018**, *88*, 504–533. [CrossRef] [PubMed]
44. Yamamoto, Y.; Olsson, M.; Hogmark, S. Three-body abrasive wear of ceramic materials. *Wear* **1994**, *174*, 21–31. [CrossRef]
45. Yaqub, T.B.; Vuchkov, T.; Bruyere, S.; Pierson, A.; Cavaleiro, A. A revised interpretation of the mechanisms governing low-friction tribolayer formation in alloyed-TMD self-lubricating coatings. *Appl. Surf. Sci.* **2022**, *571*, 151302. [CrossRef]
46. Li, X.; Wang, H.; Shi, J.; Han, B.; Ren, N. Formation mechanism and function of tribo-layers in dry sliding wear of TC11 alloy. *Surf. Topogr. Metrol. Prop.* **2021**, *9*, 015013. [CrossRef]
47. Wannaparhun, S.; Seal, S.; Desai, V. Surface chemistry of nextel-720, alumina, and nextel-720/alumina ceramic matrix composite (CMC) using XPS-A tool for nano-spectroscopy. *Appl. Surf. Sci.* **2002**, *185*, 183–196. [CrossRef]
48. Khun, N.W.; Neville, A.; Kolve, I.; Zhao, H.Y. Friction and wear of DLC coating deposited on M2 steel via μW-PECVD against 100Cr6 steel with different normal loads and sliding speeds under dry and lubrication conditions. *Tribol. Ind.* **2024**, *46*, 570–588. [CrossRef]

Disclaimer/Publisher's Note: The statements, opinions and data contained in all publications are solely those of the individual author(s) and contributor(s) and not of MDPI and/or the editor(s). MDPI and/or the editor(s) disclaim responsibility for any injury to people or property resulting from any ideas, methods, instructions or products referred to in the content.